*Desalination and Water Treatment*
www.deswater.com
doi: 10.5004/dwt.2020.25659

192 (2020) 195–212
July

# Sulfur and nitrogen doped-titanium dioxide coated on glass microspheres as a high performance catalyst for removal of naphthalene ($C_{10}H_8$) from aqueous environments using photo oxidation in the presence of visible and sunlight

Abbas Jafari[a], Mehrban Sadeghi[a,b,*], Farhang Tirgir[a,c,*], Seyed Mehdi Borghaei[d]

[a]*Department of Natural Resources and Environment, Science and Research Branch, Islamic Azad University, Tehran, Iran, Tel. +98 38333346712; Fax: +98 38333334678; emails: sadeghi@skums.ac.ir (M. sadeghi), tirgir588@gmail.com (F. Tirgir)*
[b]*Department of Environmental Health Engineering, School of Health, Shahrekord University of Medical Sciences, Rahmatieh Shahrekord, Iran*
[c]*Department of Chemistry, Faculty of Science, Shahrekord Branch, Islamic Azad University, Shahrekord, Iran*
[d]*Department of Chemical and Petroleum Engineering, Sharif University of Technology, Tehran, Iran, email: mborghei@sharif.edu (S.M. Borghei)*

Received 23 July 2019; Accepted 26 January 2020

**ABSTRACT**

Naphthalene is a toxic aromatic compound whose presence in aqueous environments is very hazardous. In this research, naphthalene removal from wastewater using titanium dioxide–nitrogen–sulfur ($TiO_2$–N–S) photocatalyst immobilized on glass microspheres was investigated. Additionally, the effect of visible and sunlight, radiation time, pH, and initial concentration of naphthalene on photocatalytic removal of naphthalene were studied. Scanning electron microscope images revealed nanoparticles with an average size between 10 and 15 nm, and X-ray diffraction pattern revealed nano-photocatalyst with an average size of 11 nm. Energy-dispersive X-ray showed the presence of two elements, that is, sulfur and nitrogen in the crystalline structure of $TiO_2$ powder, and diffuse reflectance spectroscopy showed the energy bandgap narrowing and transfer of photocatalytic activity of $TiO_2$–N–S to the visible region. Chemical kinetic equation of naphthalene removal was second-order kinetic. The maximum level of naphthalene removal in the presence of visible and sunlight was obtained at a concentration of 25 mg/L (94.29%) and 40 mg/L (93.24%), respectively. Therefore, the immobilized $TiO_2$–N–S on glass microspheres can be used as a new, effective, and functional method in treating water and industrial wastewater containing naphthalene in the presence of visible and sunlight.

*Keywords:* $TiO_2$–N–S photocatalyst; Photooxidation; Sunlight; Visible light; Naphthalene removal; Chemical kinetic

## 1. Introduction

Naphthalene is one of the polycyclic aromatic hydrocarbons (PAHs) and hazardous pollutants [1,2] with a relatively high degree of toxicity. It is one of the causes of kidney failure, congenital disorders, and biodegradation resistance. Moreover, it has been considered as a carcinogenic, mutagenic, and teratogenic pollutant by the US Environmental Protection Agency [3–5]. In polluted soils, it is very likely that these compounds make strong bonds with solid particles. At the same time, some of them can pass through the soil porous media and contaminate groundwaters. PAHs can enter the aquatic and soil environments from a number of sources, including industrial, and domestic wastewater, extraction of petroleum products, pharmacy, paint, plastic, insecticides, and petrochemical plants, heavy oil production

* Corresponding authors.

facilitates, coke furnace, and scrap tires, and can enter the human body directly [2,6–10]. Due to high-risk effects of PAHs on human health, it is essential to assess the potential of water contamination with these compounds [11]. According to the World Health Organization guideline, the allowable limit for naphthalene in drinking water is 0.05 mg/L. Therefore, naphthalene removal in aqueous environments is of paramount importance [12], and purification of aqueous solutions containing naphthalene is necessary to keep the environment safe and healthy. Among methods for removal of PAHs are adsorption on activated carbon [9,13], sand bed [14], and biomass gasifiers [15]; simultaneous application of ultrasound pretreatment and mesophilic and thermophilic anaerobic digestion [16]; anaerobic biodegradation [17]; and the use of metal catalysts [18]. In the above mentioned methods, naphthalene is only transferred from one phase to another, but it is not converted into harmless compounds [19]. Among all these methods for removing organic pollutants from water and wastewater, biological degradation of effluent using microorganisms has received more attention, but the biological removal efficiency of PAHs such as naphthalene has reduced significantly due to the presence of benzene rings in the molecule, and microorganisms cannot decompose it.

Therefore, in recent years, new advanced oxidation processes have been considered [20]. Photocatalyst removal is done by shining ultraviolet on the surface of a conductive semiconductor, such as ZnO or $TiO_2$, and oxidation is usually based on the activity of highly reactive species such as hydroxyl radicals [21–23]. Due to their eco-friendly nature and high optical activity, low price, low toxicity, and high chemical and thermal stability, heterogeneous photocatalysts such as anatase $TiO_2$ crystals are regarded as the most popular photocatalysts [24–26]. Though Titanium dioxide ($TiO_2$) powder nanoparticles have been widely used over the past 30 y, efforts to immobilize photocatalysts on surfaces such as glass spheres, glass fibers [27–29], silica [30,31], activated carbon, zeolites, and nanotubes are on the rise due to problems such as the need for continuous mixing during work, the high cost of filtration and centrifugation of solutions to recover powders, nanoparticles dispersion in solution and light blockage, etc. [25,26,32–35]. Two important advantages ensue from optical degradation of pollutants in the form of a thin film. The first one is avoiding high costs of catalyst separation, and the second is a lack of formation of dangerous compounds caused by advanced oxidation, which are often formed using other oxidants, such as halogens [36]. On the other hand, the wide bandgap of $TiO_2$ has converted it to an efficient photocatalyst in the ultraviolet region, but naturally, only 4% of sunlight is ultraviolet and photocatalytic removal of naphthalene using ultraviolet light in aqueous solutions with practical limitations, such as the short life of ultraviolet lamps and electrical energy consumption cause an increase in treatment costs, and finally, the ultraviolet lamp is considered as a serious threat to the environment [24–27]. Therefore, in order to modify this intrinsic property of $TiO_2$ and produce a new photocatalyst which is capable of keeping its photocatalytic activity in the presence of sunlight, methods such as doping with noble metals, metal ions, and anions (C, N, F, S) are being developed [37–40]. The use of earth elements such as La, Ce, Gd to create electron-hole [41–43] and co-doping with metallic and earth elements have received lots of attention. Yu et al. [44] doped N and La elements on $TiO_2$ network in order to reduce the energy band gap and increase the optical activity of $TiO_2$ in a visible light region of N and La [45,46]. Doping sulfur anions and nitrogen with $TiO_2$ makes the gap between two strips of capacity and conductivity narrower, leading to absorption in the visible region [32,47–49]. Therefore, solar photocatalytic processes are regarded as an appropriate technology that complements the physical and even biological methods of treatment [50]. Over the past years, glass microspheres application for catalyst deposition has received lots of attention [51,52]. The aim of the present research is to investigate the photocatalytic effect of immobilized titanium dioxide–nitrogen–sulfur ($TiO_2$–N–S) on naphthalene removal from aqueous solutions. The immobilized $TiO_2$–N–S nanoparticles were assayed using a scanning electron microscope (SEM) [53], X-ray diffraction (XRD), and energy-dispersive X-ray (EDX). Additionally, the optimal conditions of naphthalene removal will be studied using pH, radiation time, and concentration of naphthalene in the presence of visible and sunlight. Finally, the kinetics of the removal reactions of naphthalene will be studied.

## 2. Materials and methods

### 2.1. Photocatalyst synthesis

All chemical materials were purchased from Germany's Merck Company. In addition, deionized water was prepared in laboratory using water distillation unit of GFL Company, Germany. First, $TiO_2$ and $TiO_2$–N–S nanoparticles were synthesized using sol–gel method [54]. $TiO_2$ sol was prepared through hydrolysis of tetrabutyl orthotitanate (TBOT) in acid solution as follows: first, 2.5 mL of TBOT compound, 10 mL ethanol, and 2.5 mL acetylacetone were mixed together. After 30 min of stirring, a clear yellow solution was obtained. In fact, acetylacetone prevents from early hydrolysis of TBOT by forming chelate. In the next step, 2 mL deionized water was added to the solution and the solution was stirred by stirrer. To adjust the pH of the solution to 1.8, concentrated hydrochloric acid and sodium hydroxide were used. After that, 0.25 mg thiourea as the source of nitrogen and sulfur was added to the synthesized sol, and this solution was put in the stirrer for another 2 h to produce a stable yellow sol. In order to immobilize the prepared sol on a substrate, 500 micron in diameter glass microspheres made in Glass Beads (Pana Company, Iran) were used. First, glass microspheres were rinsed with detergent solution and put in dilute hydrochloric acid for 8 h, and dried in oven at 105°C after being rinsed with deionized water. Then microspheres were immersed in sol solution and put in the stirrer for 10 min. In the next stage, the glass microspheres were put in the oven for 4 h at 60°C and in order to remove probable contaminants, glass microspheres were rinsed in the ultrasonic bath for 30 min. Fig. 1 shows the preparation and synthesis steps of $TiO_2$–N–S catalyst.

### 2.2. Naphthalene extraction and gas chromatography–mass spectrometry analysis

In order to extract naphthalene from aqueous environment and prepare solution to be injected to GC-MS device,

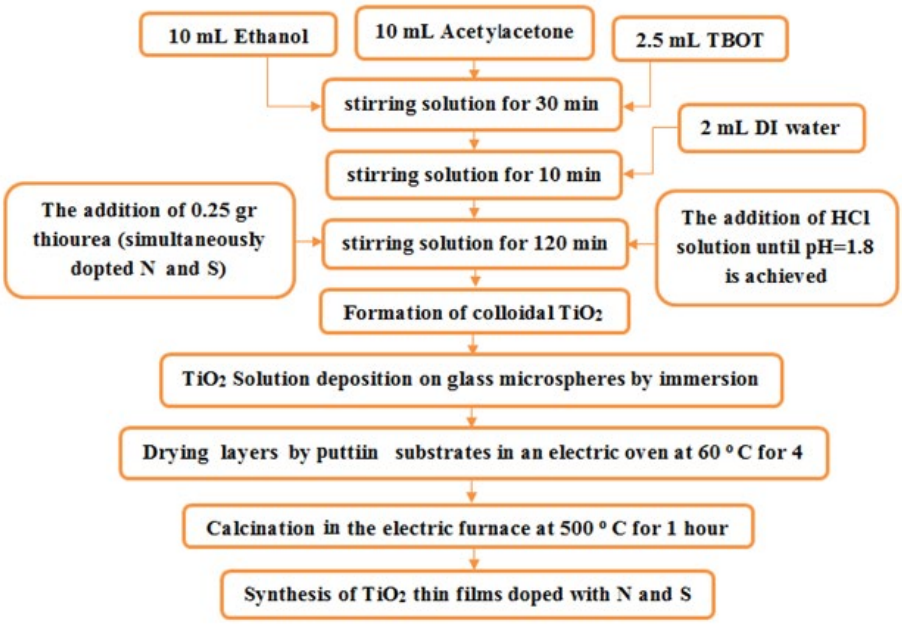


Fig. 1. Schematic diagram of $TiO_2$–N–S catalyst preparation and synthesis steps.

the following steps were done. First, 200 mL of naphthalene solution with certain initial concentration was prepared and its pH reached 2 using phosphoric acid, then 50 mL pure dichloromethane was added to the sample and it was poured into a separation funnel and stirred for 5 min, then separation funnel was put in settlement conditions for 30 min so that the solution could be fully separated into two phases. The bottom layer in the separation funnel was drained and again 25 mL dichloromethane was added and after 30 min spent in settlement conditions, the bottom layer was drained out, and the top layer of two stages were mixed together and kept in a locked container until it was injected to gas chromatography–mass spectrometry (GC–MS) device. The volume of the obtained extraction was reduced to 2 mL using a rotary evaporator, and 2 mL methanol was added to it. The sample was rotated again and 5 mL methanol was added to it once more, and samples were dried using slow flow of nitrogen gas. To ensure the removal of water from organic phase, a small amount of water-free sodium sulfate powder was added and passed through Whatman PTFE membrane filter with a diameter of 0.45 micron [55], and the sample was injected into the GC–MS. In order to identify the intermediate compounds produced by photo-oxidation reactions of naphthalene with $TiO_2$–N–S catalyst, gas chromatography (Agilent Technologies 7890A model GC) Manufactured by Agilent, USA device connected to mass spectrometer (Agilent Technologies-5975C Model) Manufactured by Agilent, USA with a 30 m in length HP5-MS column with outer diameter of 0.25 m, and inner diameter of 0.25 μm was used. The ion capacity of the device and initial oven temperature was 70 eV and 50°C, respectively. The sample was kept at this temperature for 2 min. The temperature was increased up to 280°C with a rate of 4°C/min. Helium gas was used as a carrier gas at a flow rate of 2 mL/min. The prepared sample was injected into the GC–MS at a volume of 0.1 μl [56,57].

### 2.3. Study of photocatalyst properties

The bandgap of $TiO_2$–N–S photocatalyst was obtained using ultraviolet-visible (UV-Vis) reflection spectroscopy through AVASPEC 2048 Tech (AVANTES Company) spectrophotometer and Eq. (1) [58].

$$E_g = \frac{1,238.9}{\lambda} \tag{1}$$

where $\lambda$ is the wavelength of absorption layers in the spectrum in nanometer, and $E_g$ is the bandgap in terms of eV. XRD analysis was performed to determine polymorphs and size of $TiO_2$ film crystals on glass spheres using X'Pert Pro MPD (PANalytical, The Netherlands) device in the range of $2\theta = 10°–80°$. The average size of crystalline particles of the anatase phase was estimated by Sherer's Eq. (2) [59].

$$S = \frac{K\lambda}{\beta\cos\theta} \tag{2}$$

where $S$ is the mean size of crystalline dimensions, $k$ is the shape factor of crystal particles (0.89), $\theta$ is the diffraction angle at the maximum peak, $\lambda$ is the X-ray wavelength, and $\beta$ is the peak broadening at half of its height in radians [60]. The surface morphology of $TiO_2$ and $TiO_2$–N–S film was investigated using (SEM) Tescan MIRA3 (Tescan, Czech Republic) equipped with XRD spectrometer for element analysis.

### 2.4. Study of photocatalyst optical activity

Using sol–gel synthesized $TiO_2$ solution doped with sulfur and nitrogen on glass microspheres, the photocatalytic thin film was prepared and its effect on naphthalene removal from artificial aqueous environments was investigated. The

thickness of the thin layer coated on glass microspheres was obtained to be 865.98 nm in $TiO_2$ thin film and 698.98 nm in $TiO_2$–N–S thin film based on the results of EDX and SEM analysis, respectively. The glass microspheres were distributed in four phototubes made of quartz with an inner diameter of 0.8 cm and a height of 20 cm. Using 4.5 g glass microspheres, a specific surface area of about 0.5 $m^2/g$ was assigned to each phototube. The glass tubes were immobilized on a mirror. Fig. 2 shows the reactor used for a photocatalytic experiment

Five hundred milliliters of naphthalene solution was rotated in a closed reactor with a flow rate of 20 mL/min using a peristaltic pump. The glass tubes filled with glass microspheres were exposed to visible light using a 400 W lamp source in a dark chamber (70 cm × 70 cm × 100 cm) and sunlight. The distance between lamp and glass tubes in the dark chamber was 20 cm. In order to keep the temperature constant at 30°C inside the reactor, a cooler pump and a cold water tank connected to faucet were used. The maximum temperature in the dark chamber was reported to be 40. The initial concentrations of naphthalene solution were chosen to be 5, 10, 15, 20, 25, 40, 45, and 50 mg/L, and each concentration was tested for 4 h.

The solubility of naphthalene in water is a function of the solution temperature and its solubility is 31.6 mg/L at 25°C. As the temperature of the reservoir containing naphthalene solution is 30°C, as well as the interior temperature of the dark chamber, is 40°C due to the lamp heat, naphthalene solution was made without naphthalene solvent at a concentration up to 25 mg/L. in order to make naphthalene solution at concentrations of 40, 45, and 50 mg/L, methanol solvent was used. A total volume of 150 mg/L naphthalene was solved in 45 mL methanol. It was then dissolved in distilled water and diluted to 4,500 mL and used to prepare different concentrations of this solution [61–63]. The solutions were made for at least three repetitions for each concentration and only one catalyst substrate was used for all three repetitions. After each use, the catalyst was washed several times with distilled water, ultrasonicated, and oven-dried at 100°C for 90 min and reused.

In order to adjust pH, NaOH, and hydrochloric acid were used. The residual concentration of naphthalene solution was measured at a maximum wavelength of 276 nm using the Uv-Vis Spectrophotometer made in America (Perkin Elmer) [64] and naphthalene degradation efficiency was calculated using Eq. (3).

$$\eta = \frac{C_0 - C_t}{C_0} \times 100 \tag{3}$$

where $C_0$ is the initial concentration and $C_t$ is the residual concentration of naphthalene after time $t$, and η is the naphthalene removal percentage. All experiments were done triplicate and the mean value was reported.

### 2.5. Statistical analysis

In order to determine the experiments accuracy, one-way analysis of variance was used. Additionally, Tukey test was used to determine $p$-value and the standard deviation.

## 3. Results and discussion

### 3.1. Photocatalyst properties

The XRD patterns of $TiO_2$ and $TiO_2$–N–S powder and $TiO_2$–N–S as thin film coated on glass microspheres are shown in Figs. 3a–c, respectively. Figs. 3a–c show diffraction pattern of titanium elements in synthetic photocatalyst as anatase phase. The XRD pattern of pure glass microspheres shows the amorphous solid (as a blank) (Fig. 3d). The average size of crystal nanoparticles in the $TiO_2$–N–S thin film doped on glass microspheres at peak 101 (according XRD pattern) was calculated to be 11 nm using Sherer's equation, and 14 nm for $TiO_2$ thin film coated on microspheres, respectively. From the result, characteristic peak at 2θ = 25.348 was obtained that represent anatase phase (JCPDS file number = 01-089-4921). There is no trace of rutile and brookite phases. XRD results of this research are in close agreement with those obtained by Sathish et al. [65] and Brindha et al. [66]. They reported the

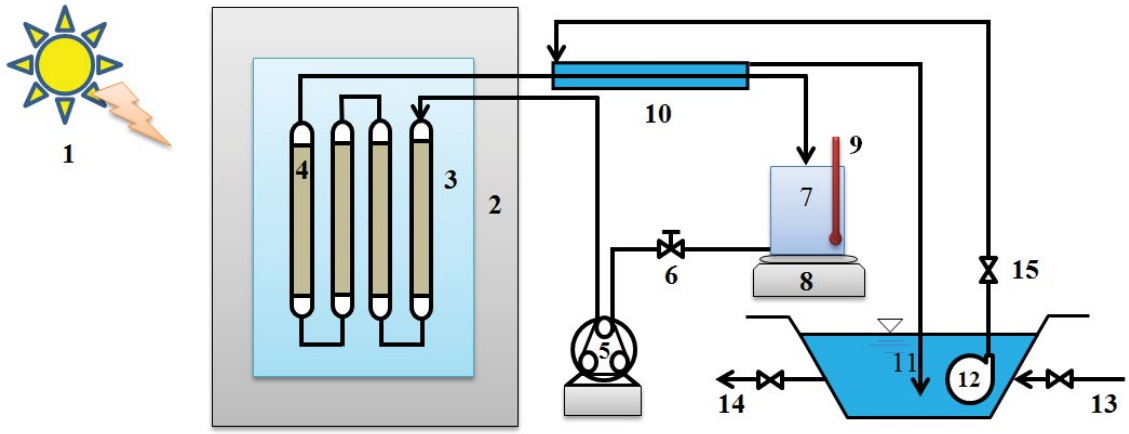


Fig. 2. Schematic diagram of the pilot. (1) Sunlight, (2) wooden support plate, (3) mirror, (4) Photoreactor containing glass microspheres, (5) peristaltic pump, (6) sampling valve, (7) basin containing naphthalene solution, (8) magnetic stirrer, (9) alcoholic thermometer, (10) condenser, (11) water basin, (12) pump, (13) clean water, (14) effluent, and (15) cut-off valve.

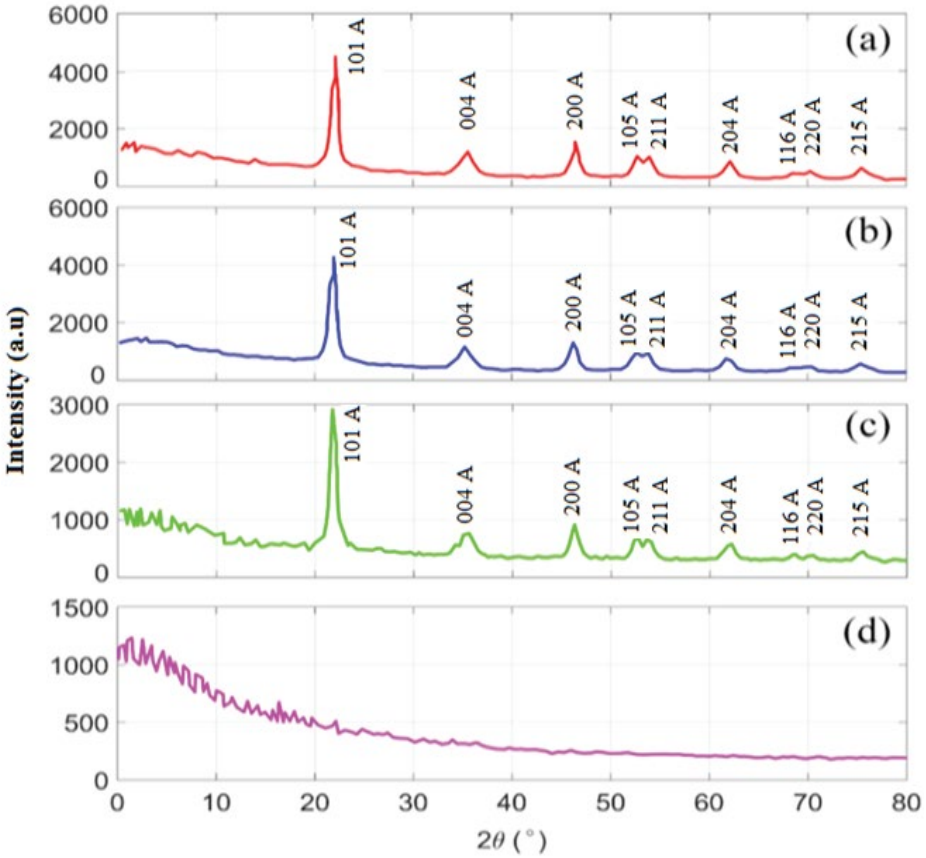


Fig. 3. XRD pattern of thin film. (a) Image of phase structure and crystal size of $TiO_2$ powder, (b) image of phase structure and size of $TiO_2$–N–S powder, (c) image of $TiO_2$–N–S thin film doped on glass microspheres, and (d) non-coated (pure) glass microspheres.

diameter of $TiO_2$–N–S nanoparticles to be 15 nm at the temperature of 500°C, which is close to the size of nanoparticles (14 nm) in this research.

The SEM images of pure glass microspheres and $TiO_2$ thin film coated on glass microspheres are shown in Figs. 4a and b, respectively. Figs. 4c and d respectively display the $TiO_2$ thin film coated on the glass microspheres and the thickness of this $TiO_2$ thin film, which is equal to 809.93 nm. Figs. 4e and f, respectively, display the uniform $TiO_2$ thin film coated on the glass microspheres and the thickness of the $TiO_2$–N–S thin film, which is equal to 639.68 nm. Figs. 4g and h illustrate the nano size of $TiO_2$–N–S particles in thin film, which is estimated to be 10–15 nm, and the accumulation of nanoparticles, respectively. The results are also confirmed by the XRD technique. Generally, the nanoparticles of phtocatalyst coated on glass microspheres tend to accumulate beside each other due to the van der Waals interaction between the surfaces of the particles [20]. This is displayed in Figs. 5a and d.

According to Fig. 5, elemental analysis of thin-film $TiO_2$ coated on glass microspheres indicates 45.1 wt.% oxygen, 35.3 wt.% silicon, 8.6 wt.% sodium, 2.4 wt.% magnesium, 7.4 wt.% calcium (which is related to glass microspheres), and 1.2 wt.% titanium, and lacks sulfur and nitrogen. The thin-film $TiO_2$–N–S coated on glass microspheres indicates 42.2 wt.% oxygen, 7.78 wt.% silicon, 2.53 wt.% sodium, 0.84 wt.% magnesium, 2.34 wt.% calcium, 34.71 wt.% titanium, 10.92 wt.% nitrogen, and 0.68 wt.% sulfur, indicating that the new photocatalytic layer contains doped nitrogen and oxygen atoms.

In order to investigate elemental analysis, and to calculate the weight percent and atomic percent of the elements existing on the surface of the sample, EDX analysis was used. Fig. 5 illustrates EDX analysis of $TiO_2$ and $TiO_2$–N–S thin film on glass microspheres and its corresponding SEM images. Fig. 5b shows the peaks of thin layer $TiO_2$ coated on glass microspheres which confirm the presence of Ti and Si without the presence of N and S in the structure of the thin film of $TiO_2$. It should be noted that the elements of Mg, Na, and Ca in the EDX analysis spectrum are related to the glass microspheres structure. Fig. 5d shows EDX analysis related to $TiO_2$–N–S thin film (corresponding to its SEM image (Fig. 4c)). The peaks related to the presence of sulfur and nitrogen are at 0.5 and 3.2 K eV, respectively. Ti peak is observed at about 1.5–8.5 K eV. The more intense peak is related to the internal $TiO_2$, which can be clearly observed in Fig. 5d.

### 3.2. Photocatalyst optical properties

FT-IR spectrum of $TiO_2$–N–S powder samples at 60°C and $TiO_2$–N–S at 500°C are shown in Figs. 6a and b,

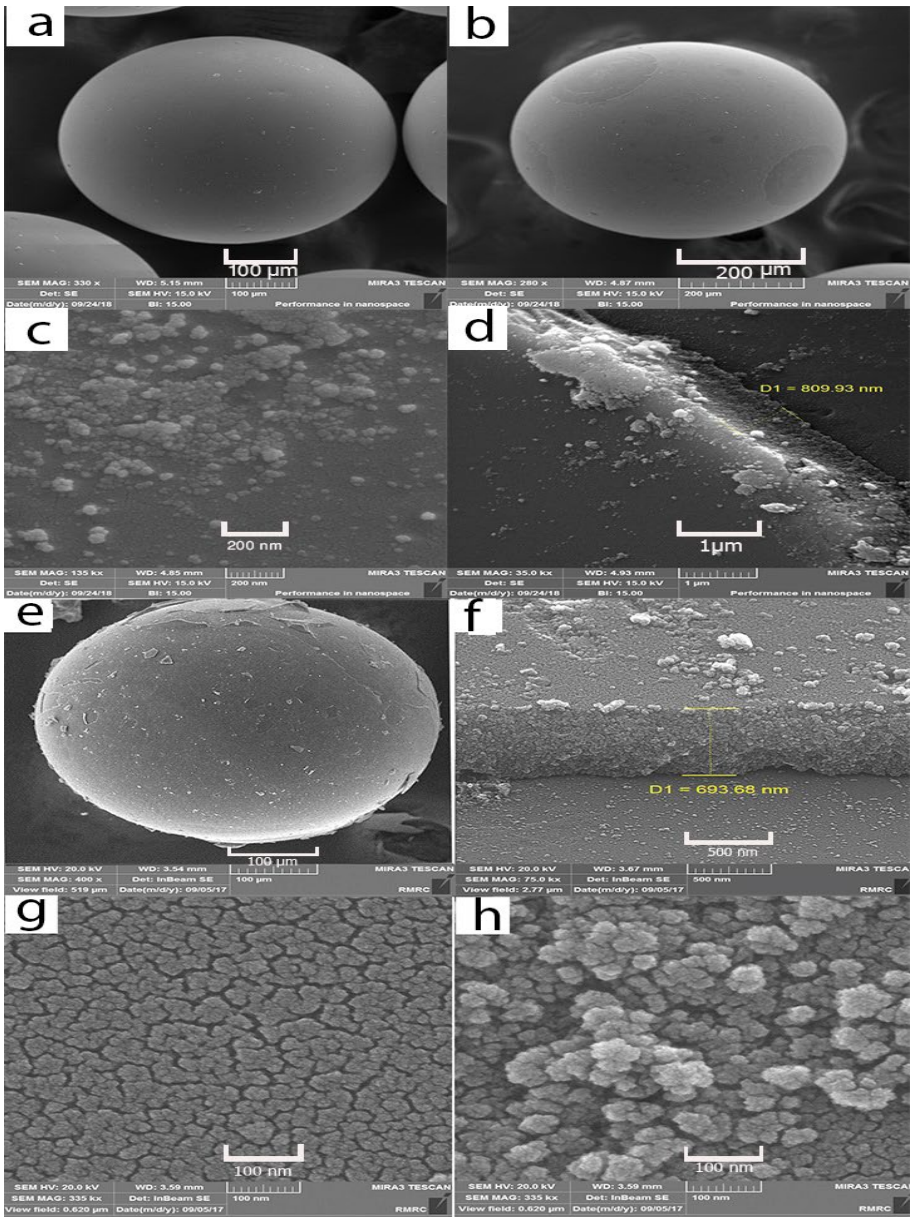


Fig. 4. SEM images of $TiO_2$ and $TiO_2$ doped with nitrogen and sulfur on glass microspheres. (a) Image of non-coated glass microspheres, (b) image of glass microspheres coated with $TiO_2$ thin film, (c) image of $TiO_2$ nanoparticle coated on the surface of glass microspheres, (d) thickness of $TiO_2$ thin film coated on the glass microspheres surface, (e) uniform $TiO_2$–N–S thin film coated on the glass microspheres surface, (f) nanometer sized thickness of $TiO_2$–N–S thin film, (g) high resolution image of nanometer sized $TiO_2$–N–S particles on the glass microspheres surface, AND (h) high-resolution image of nanometer sized $TiO_2$–N–S particles on the surface of glass microspheres from another angle.

respectively. Fig. 6a that shows the absorption spectrum at 3,300–3,180 $cm^{-1}$ is related to $NH_2$ group stretching vibration of thiourea structural unit added to tetramethyl orthotitanate sol solution. Two absorption bands in the region of 1,528 and 1,587 $cm^{-1}$ are related to the stretching vibration C=S functional group of thiourea structural unit. The absorption band of bending vibration of C–O hydroxy group and C–N bond in titanium dioxide is shown at 1,280 and 1,359 $cm^{-1}$. The absorption band at 1,050 $cm^{-1}$ is related to the Ti–O–Ti band stretching vibration, showing condensation reaction between hydroxy titanium groups of tetramethyl or thotitanate reagent during hydrolysis reaction of $TiO_2$ nanoparticles, and finally, its presence on $TiO_2$ nanoparticles modified by S and N. Fig. 6b displays FT-IR spectrum of $TiO_2$–S–N nanoparticles spectrum formed at 500°C for 1 h. The absorption band of $TiO_2$ hydroxy group stretching vibration has been much broadened at 3,000–3,423 $cm^{-1}$ due to the existence of different hydroxyl groups in different sites, as well as the number of different interactions in terms of the number of hydrogen bonds between hydroxy groups. The vibration band at 540–643 $cm^{-1}$ is allocated to Ti–O–Ti band stretching vibration of fuzzy network anatase and

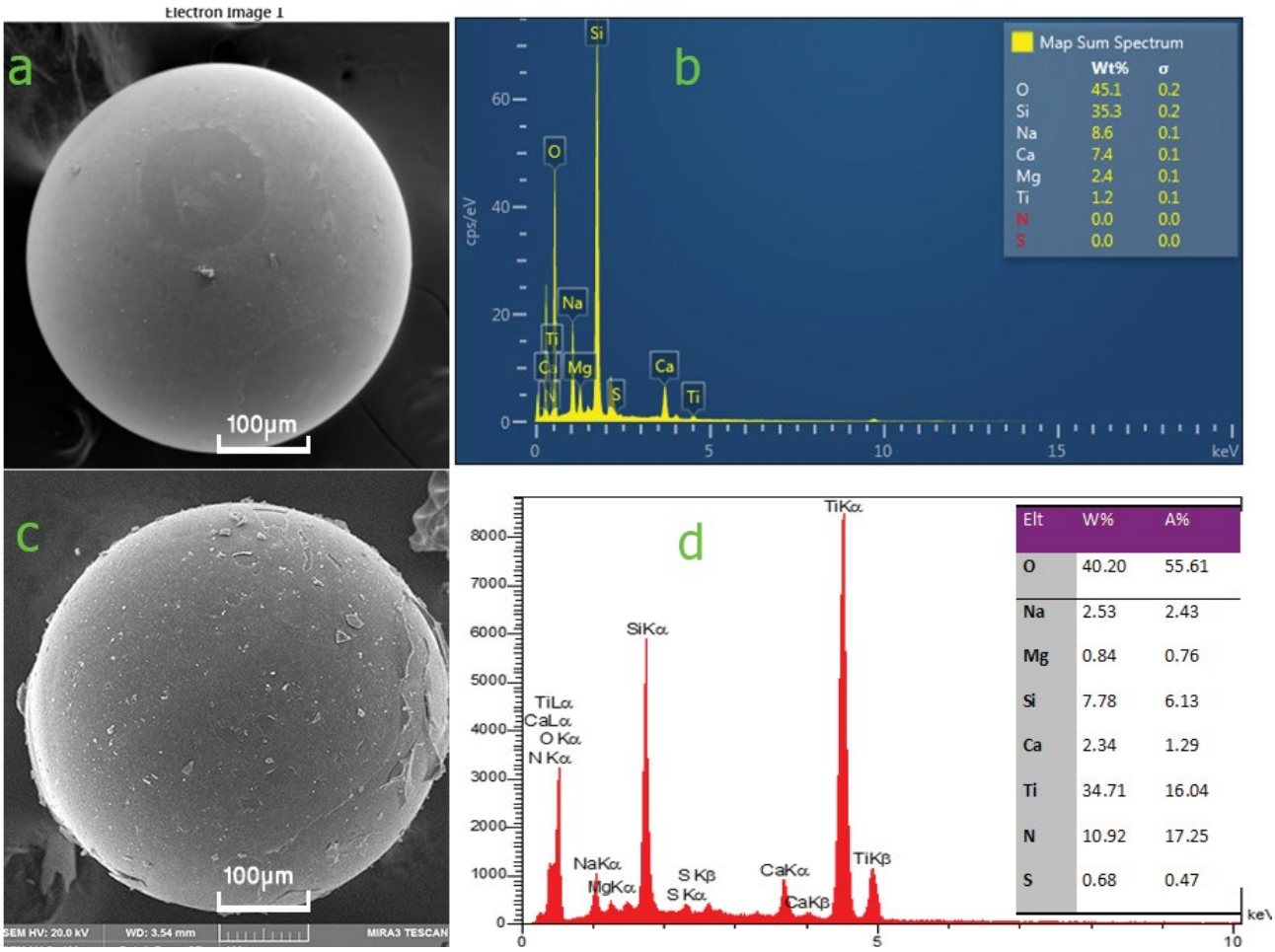


Fig. 5. EDX spectrum and SEM images related to $TiO_2$ and $TiO_2$–N–S coated on glass microspheres, respectively, (a) SEM image of $TiO_2$ thin film on glass microspheres, (b) EDX analysis related to $TiO_2$ coated on glass microspheres, (c) SEM image of $TiO_2$–N–S thin film on glass microspheres, and (d) EDX analysis related to $TiO_2$–N–S thin film together with glass microspheres.

increases better oxidation of photocatalyst by producing OH free radicals [67–69]. Fig. 6c illustrates FT-IR spectrum of pure $TiO_2$ at 500°C for 1 h.

Diffuse reflectance spectroscopy (DRS) spectrum of $TiO_2$ and $TiO_2$–N–S thin film on glass microspheres is shown in Fig. 7. UV-Vis DRS spectrum analysis of pure $TiO_2$ and $TiO_2$ doped with sulfur and nitrogen is displayed in Fig. 7. As shown, the value of diffusion coefficient of $TiO_2$–N–S spectrum in visible region is stronger than $TiO_2$. In order to estimate the optical band-gap energy of nanostructures, Tauc plot method (Tauc) was used. In this method, the relation known as Kubelka–Munk model is used [70]. The amount of absorption obtained for $TiO_2$ thin film and $TiO_2$–N–S thin film was 378 and 416 nm, respectively. These values were calculated respectively to be equal to an energy gap of 3.2 eV for $TiO_2$ thin film and 2.98 eV for $TiO_2$–N–S thin film. This was in agreement with that obtained by Appavu et al. [66,71]. As it can be observed, the effect of the addition of two nonmetal elements of sulfur and nitrogen in the crystalline structure of $TiO_2$ powder made the gap energy narrower and transferred photocatalytic activity of $TiO_2$ to visible region [53]. This energy gap is narrower than mixing of p and nonmetal and 2p orbitals of oxygen in $TiO_2$ [46,72,73].

### 3.3. Determining purity percentage of naphthalene

In order to determine purity percentage of naphthalene crystal, Agilent 7890A model GC–MS was used. The GC grade N-hexane solvent was used to extract and solve naphthalene solid crystal. After removing the *n*-hexane solvent peak in GC–MS, only one peak was observed whose spectrum was related to naphthalene ($m/z$ = 128) at retention time (RT) 13.269 min (Fig. 19a) and the MS pattern of naphthalene was shown in Fig. 19b.

### 3.4. Naphthalene removal using synthesized photocatalyst

At first, solutions with a constant concentration of 5 mg/L naphthalene were prepared at a temperature of 30°C and pHs of 3, 5, 7, 9, and 10. At each pH, 500 mL of naphthalene solution was tested in pilot of Fig. 1. After investigating and making a comparison between absorption spectrum of samples using spectrophotometer, the greatest

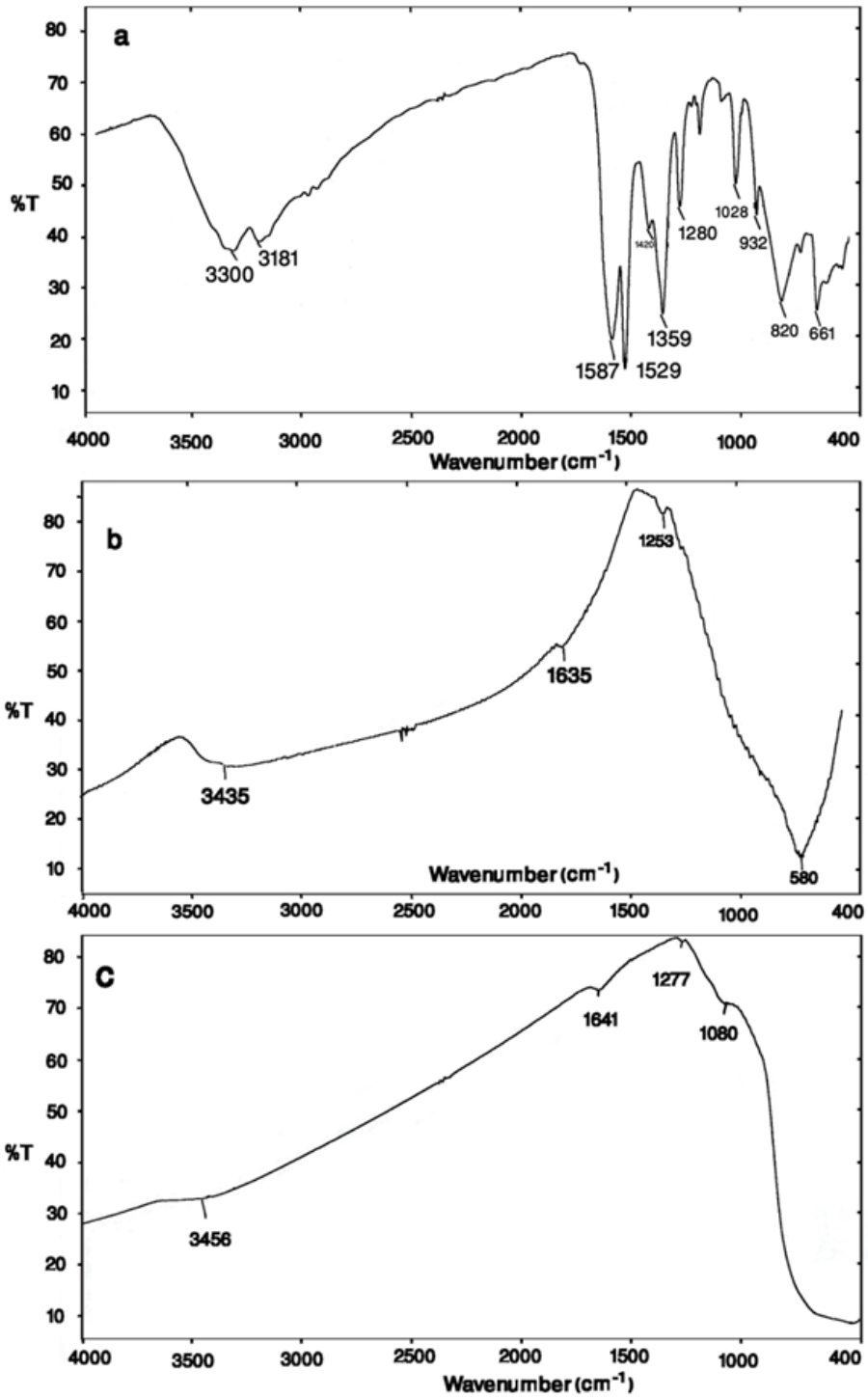


Fig. 6. (a) FT-IR spectrum of $TiO_2$–N–S at 60°C for 4 h, (b) FT-IR spectrum of $TiO_2$–N–S at 50°C for 1 h, AND (c) FT-IR spectrum of pure $TiO_2$.

efficiency of naphthalene removal was obtained at optimal pH of 5. Results are shown in Fig. 16. Then at constant pH of 5, naphthalene solutions were made with concentrations of 5, 10, 15, 20, 25, 40, 45, and 50 mg/L. In Fig. 8, considering the rate constant $K$ and $R^2$ of oxidation reaction and removal of naphthalene at pH = 5, the greatest concentration of naphthalene removal at the presence of visible light was obtained at a concentration of 25 mg/L ($pv < 0.05$). Additionally, by investigating the adsorption peaks spectrum of naphthalene solution, it was observed that from 90 min onward, another adsorption peak is emerged whose adsorption peak and spectrum is completely different from

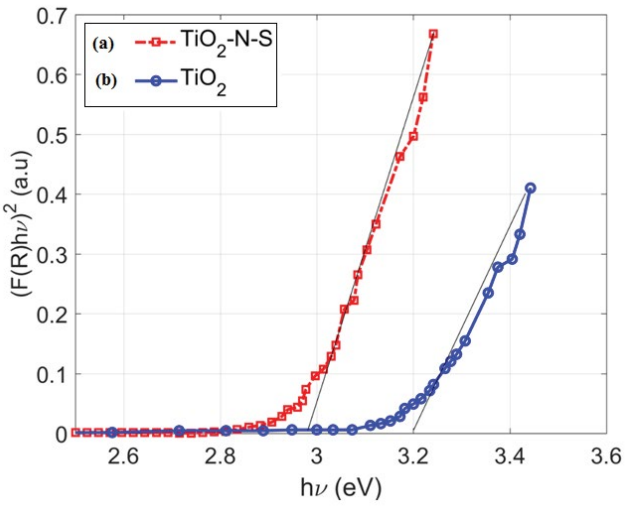


Fig. 7. DRS spectrum of $TiO_2$ and $TiO_2$–N–S thin film on the glass microspheres; DRS spectrum of (a) $TiO_2$ (blue line) and (b) $TiO_2$–N–S (red line) thin film on the glass microspheres.

naphthalene adsorption peak. Therefore, naphthalene solution samples were injected into GC–MS system from 90 min onward. It turned out that naphthalene molecule has been converted into another intermediate compound from 90 min onward. Therefore, the optimal time for naphthalene removal using this photocatalyst was assessed within 90 min, which was consistent with the result of statistical analysis (pv < 0.05). As shown in Figs. 9 and 11, the kinetics of the naphthalene oxidation and removal was assessed up to optimal time of 90 min. Considering Fig. 10, the greatest efficiency of naphthalene in the presence of sunlight was also obtained at a concentration of 40 mg/L.

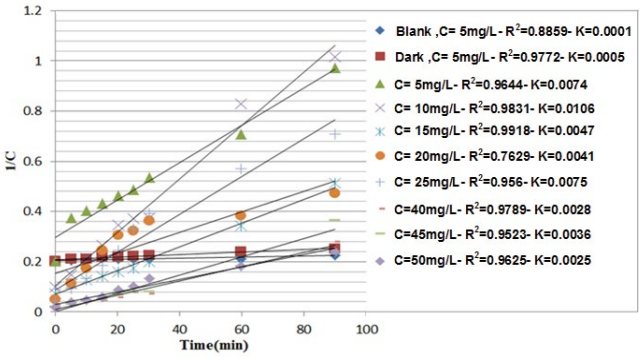


Fig. 9. Kinetic curve of the second-order equation for naphthalene degradation at different concentrations in the presence of $TiO_2$–N–S photocatalyst under visible light.

### 3.5. Effect of pH on efficiency of naphthalene removal

In order to investigate the effect of pH on the efficiency of naphthalene removal in the presence of visible light, samples with an initial concentration of 5 mg/L naphthalene solution were prepared at pHs of 3, 5, 7, 9, and 10, and samples were taken and tested at time intervals of 0, 30, 60, 90, 120, 180, 210, and 240 min. Then based on the standard method, the adsorption rate of the samples was read at wavelength of 276 nm using spectrophotometer and the percentage of naphthalene removal was calculated by Eq. (3). According to Fig. 12, the highest efficiency of naphthalene removal was obtained to be 79.04 at pH = 5 and within 90 min, which had a significant difference with other pHs within this time period (pv < 0.05), indicating that naphthalene degradation rate has increased by decreasing the solution pH. It is worth mentioning that the solution pH indicates the surface charge characteristic of photocatalyst such that in the

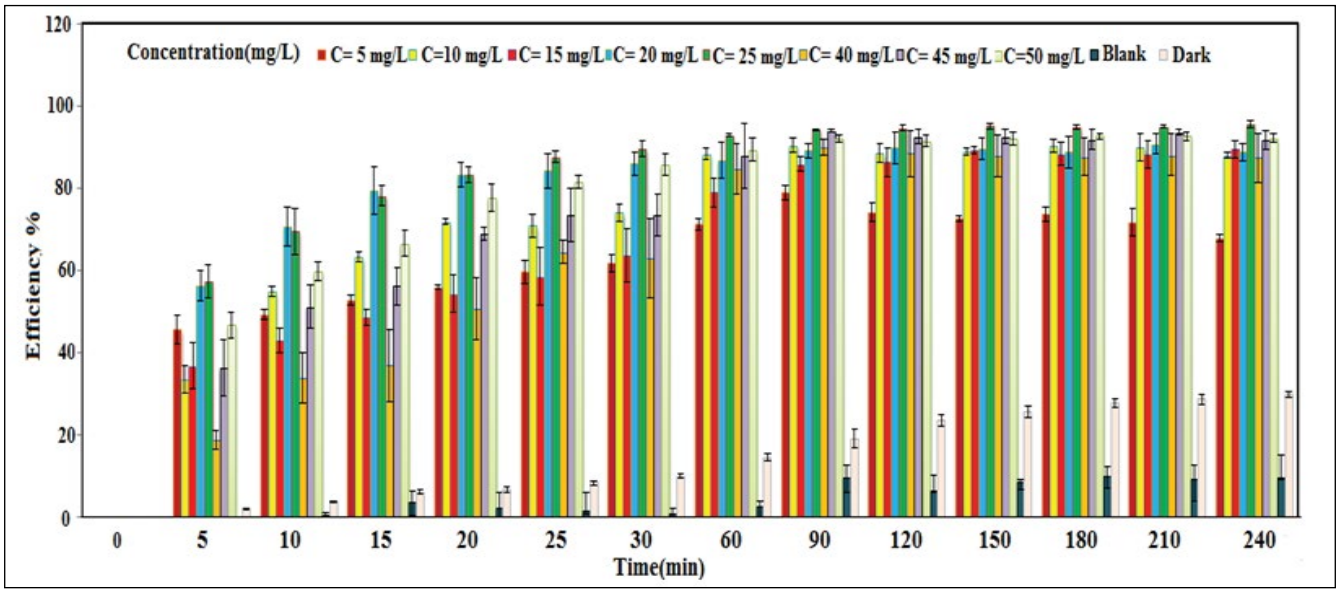


Fig. 8. Efficiency of optical degradation of naphthalene at different initial concentrations in the presence of photocatalyst under visible light within 240 min.

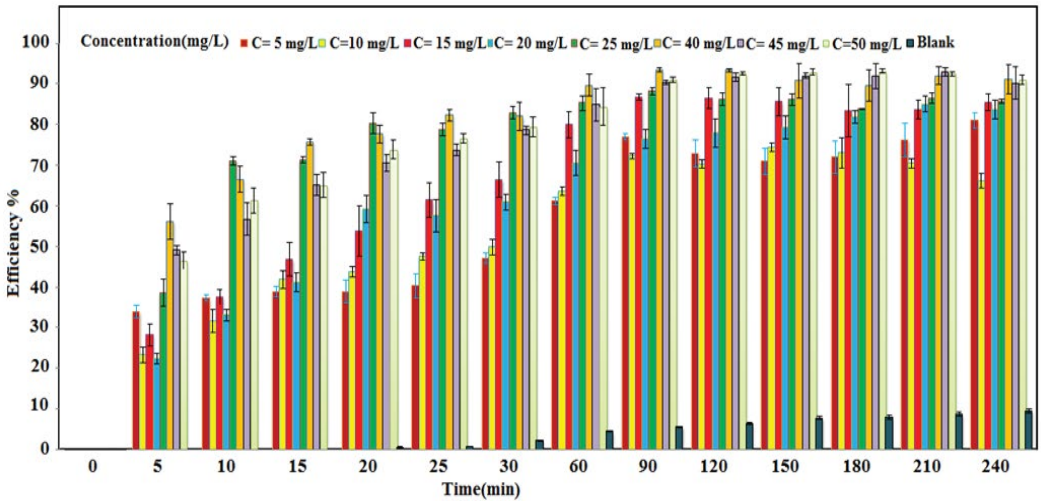


Fig. 10. Efficiency of optical degradation of naphthalene with different initial concentrations in the presence of photocatalyst under sunlight.

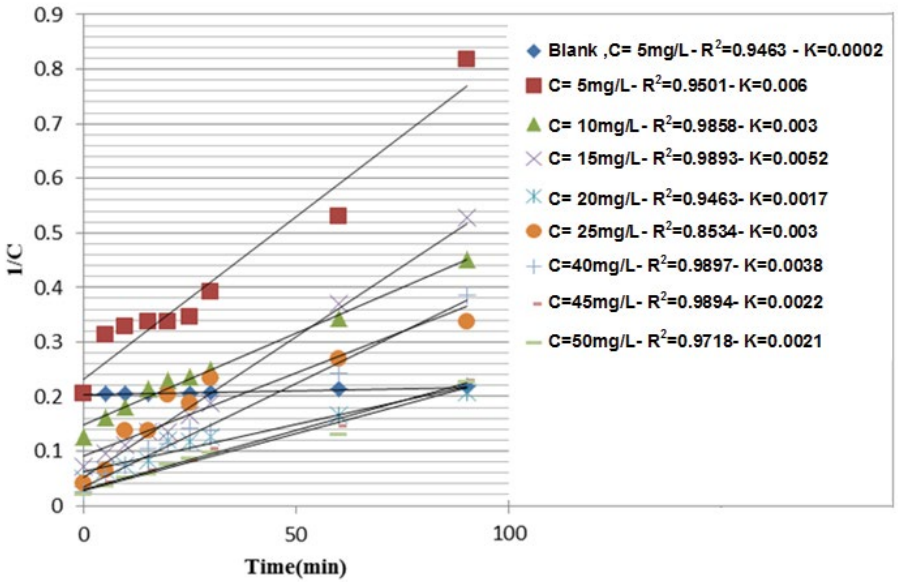


Fig. 11. Kinetic curve of the second-order equation for naphthalene degradation at different concentrations in the presence of $TiO_2$–N–S photocatalyst under sunlight.

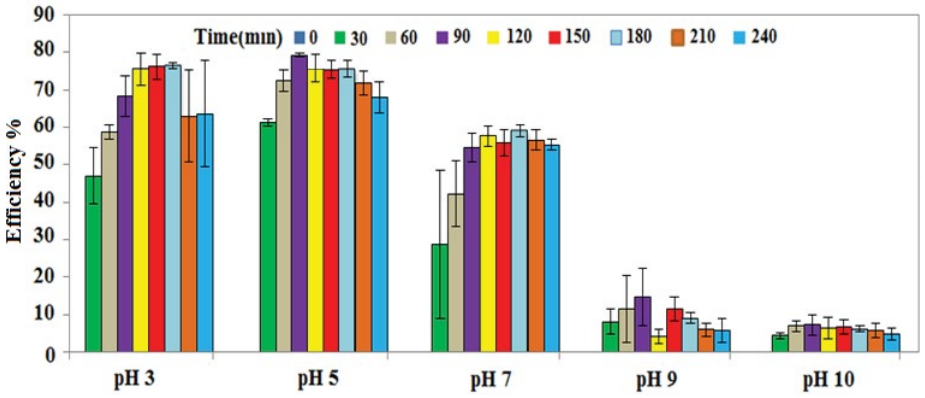


Fig. 12. Effect of pH on efficiency of naphthalene removal (pH = 5, pv < 0.05).

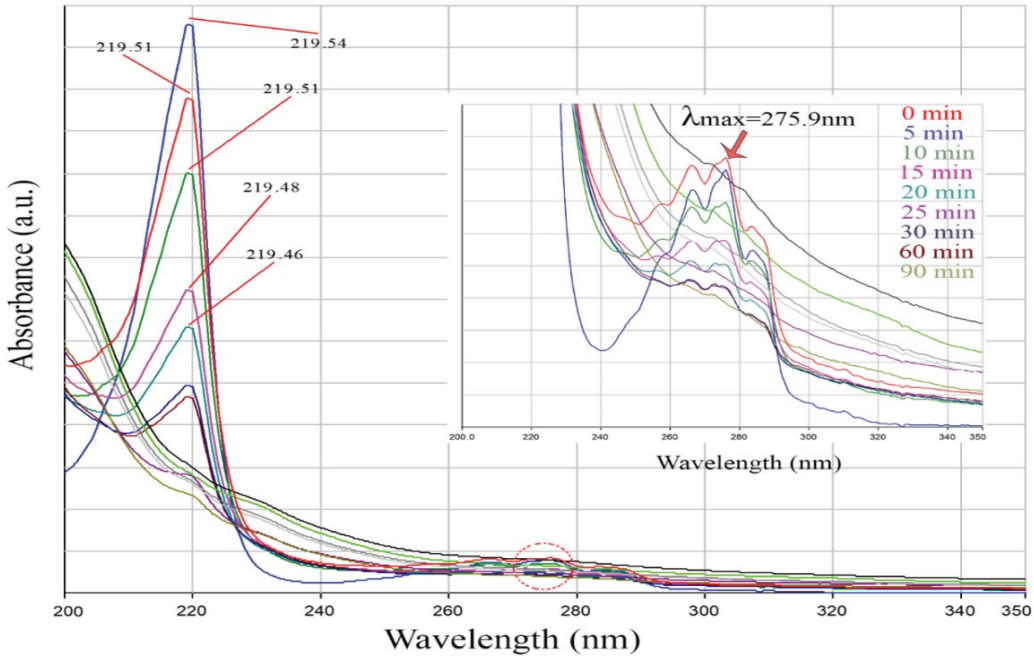


Fig. 13. UV-Vis spectrum of naphthalene solution samples under photocatalyst degradation reaction at certain times: pH = 5, naphthalene concentration = 5 mg/L under sunlight.

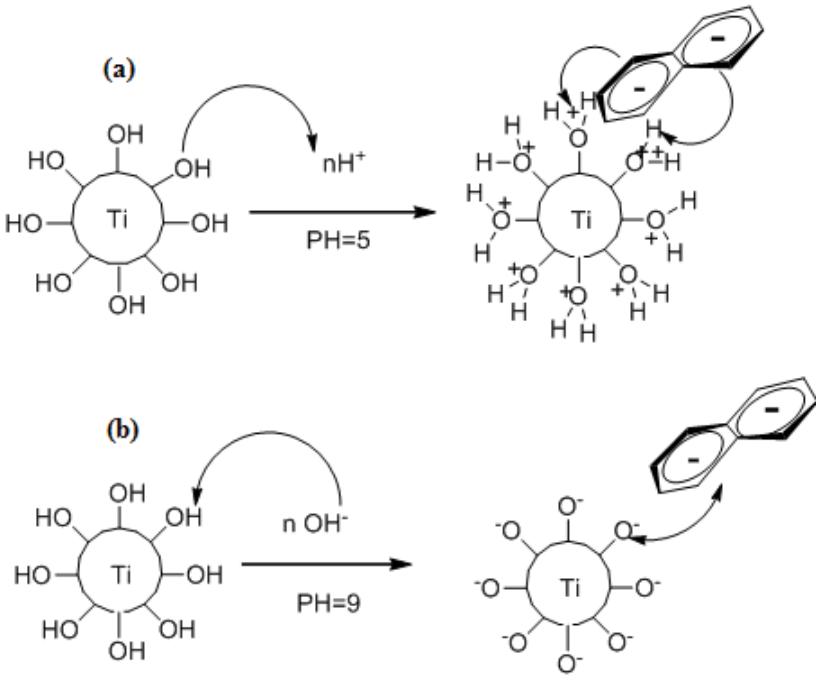


Fig. 14. The point of zero charge (pzc) of $TiO_2$ molecule was reported to be at pH 6.25. Therefore, $TiO_2$ surface will be positively charged in acidic state (a), and under weak alkaline conditions, that is, pH > 6.25, the surface charge of $TiO_2$ particles will be negative (b) [81].

acidic and basic pH values, the given photocatalyst particles carry positive and negative surface charge, respectively. The surface of $TiO_2$ catalyst in the aqueous solution is neutral at pH = 6 and its surface carries positive and negative charge at pHs below and above 6, respectively [74,75]. Zhao et al. [76] reported that the positive surface charge of $TiO_2$ has caused the produced optical electrons to better migrate at pH less than 6 and prevents recombination of electron and cavity, this way, increases the efficiency of photocatalytic process.

Fig. 13 displays overlay UV-Vis spectrum of naphthalene concentration reduction within 240 min (0–240). It is

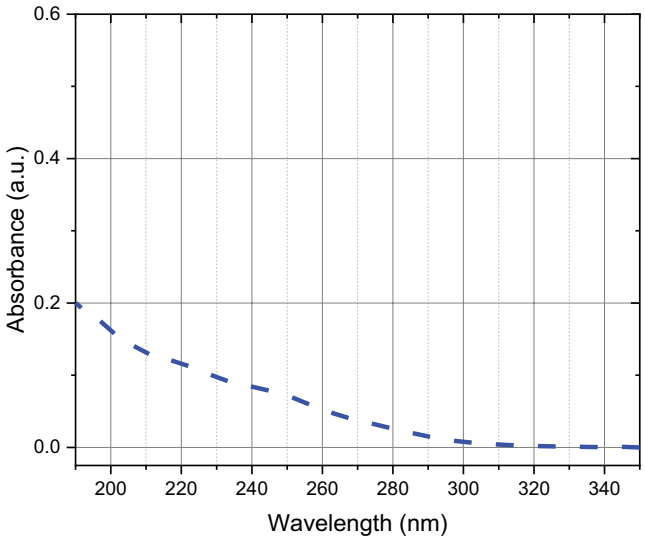


Fig. 15. UV-Vis spectrum of solution obtained from glass microspheres coated by $TiO_2$–N–S catalyst after irradiation.

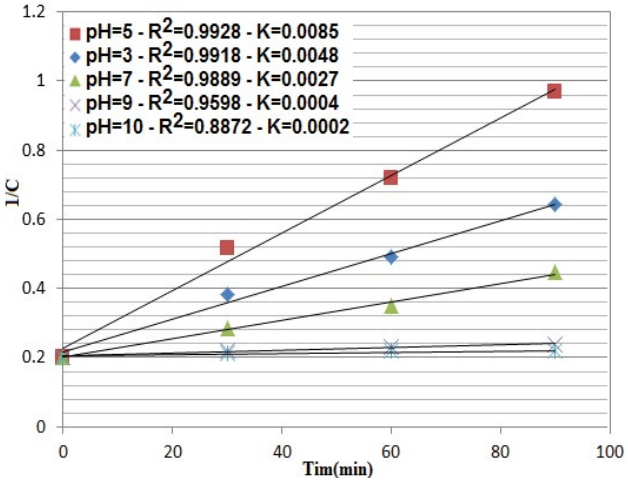


Fig. 16. Kinetic curve of second-order equation for naphthalene degradation at initial concentration of 5 mg/L at different pHs under visible light.

worth mentioning that naphthalene has two maximum wavelengths of 219 and 276 nm (Fig. 13). All of the results in kinetic calculations between absorption and concentration have been carried out at the wavelength of 276 nm because the linear relationship of Beer–Lambert law holds a link between the absorption and concentration of naphthalene at the wavelength of 276 nm, and there is no linear relationship between concentration and adsorption at the wavelength of 219 nm. In many reports, the kinetic reaction of photo-oxidation degradation of naphthalene has been reported at a maximum wavelength of 276 nm [77].

Accordingly, since 90 min onward, the shape of spectrum changes in general, indicating the production of other products except for naphthalene. In order to identify these compounds, samples were injected to GC–MS.

According to Figs. 12, 13, and 16, as the solution pH decreases, acidic condition (pH = 5) becomes dominant, and the efficiency of naphthalene increases in the presence of $TiO_2$–N–S nanocatalyst. In alkaline pH, the efficiency of naphthalene removal is significantly reduced. This indicates that naphthalene is not stuck in oxidation trap on the surface of nanocatalyst. Due to the multiple effects of pH on the surface of semiconductor $TiO_2$–N–S, molecules solubility, and radical ion formation, it is difficult to interpret the effect of pH on photocatalytic process, but in ionization mode, the photocatalyst surface can gain or lose proton under acidic and alkaline conditions based on the following relations.

According to Fig. 14, as naphthalene is negative charge due to having two benzene rings containing three double independent bonds, it can easily be absorbed on titanium oxide, which has a positive surface charge and is easily exposed to the photo-oxidation process, but as under the base conditions, $TiO_2$ surface is negatively charged, naphthalene and $TiO_2$ repel each other.

Therefore, the efficiency of naphthalene removal in acidic environment is higher due to the increased rate of hydroxyl radicals formation and adsorption on surface of $TiO_2$–N–S particles. Under alkaline pH, the possibility of surface adsorption increases due to the difference in surface charge of naphthalene molecule and $TiO_2$–N–S particles, and part of naphthalene removal in acidic pH can occur as a result of it. Over time, hydroxyl radicals, which are better formed in acidic environment, increase the removal efficiency due to oxidation effect of creating electron cavity [78–80].

According to Fig. 15, after 120 min of irradiation, the absorption of ultrasonicated solution was measured, and no absorption peak appeared in the UV-Vis spectrum of the solution. Therefore, naphthalene has not been adsorbed onto the thin layer of $TiO_2$–N–S, and naphthalene removal mechanism has been based on oxidation. The study conducted by Avisar et al. [78] on sulfamethoxazole (SMX) treatment using pH induced UV showed that an increase in pH from 5 to 7 can reduce SMX degradation [82].

### 3.6. Kinetic of photocatalytic degradation of naphthalene

The kinetic of naphthalene degradation by $TiO_2$–N–S photocatalyst was found to obey the quadratic Eq. (4).

$$\frac{1}{C_t}-\frac{1}{C_0}=Kt \tag{4}$$

where $t$, reaction time in minutes; $K$, reaction rate constant in terms of 1/min; and $C_0$ and $C_t$, initial and secondary concentration of naphthalene after the reaction in mg/L at $t = 0$ and $t = t$, respectively.

Fig. 16 shows kinetic of photocatalytic removal of naphthalene reactions and reactions rate constant and correlation coefficients from 0 to 90 min. The $K$ value of naphthalene degradation at optimal pH of 5 within 90 min is equal to 0.0085 and at a pH of 10 is equal to 0.0002. Therefore, the reaction rate of naphthalene degradation is higher in acidic pHs.

In this study, two first and second-order kinetic models were investigated for naphthalene removal. The kinetics experiments were performed by changing the contact time

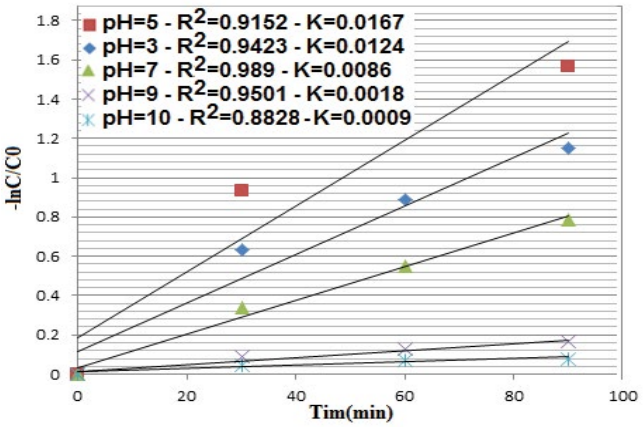


Fig. 17. Kinetic curve of the first order equation for naphthalene degradation at initial concentration of 5 mg/L at different pHs under visible light.

up to 90 min with an initial concentration of 5 mg/L naphthalene in the presence of $TiO_2$–N–S catalyst. Correlation coefficient was used to show how well the regression equation of samples fits the data. The kinetic model of naphthalene removal was analyzed by making a comparison between $R^2$ coefficients of all samples using Excel software. The second-order kinetic model of naphthalene photocatalytic removal and reaction rate constant, $k$, and correlation coefficients, $R^2$, up to 90 min at pH values of 3, 5, 7, 9, and 10 are shown in Fig. 16. The values of $K$ and $R^2$ obtained from naphthalene degradation at optimum pH of 5 within 90 min were obtained to be 0.9928 and 0.0085, respectively, and at pH 10 these values were equal to 0.8872 and 0.0002, respectively. Therefore, the reaction rate of naphthalene degradation is higher at acidic pHs. The first-order kinetic model of naphthalene photocatalytic removal at a concentration of 5 mg/L naphthalene and pH values of 3, 5, 7, 9, and 10 within 90 min is shown in Fig. 17. The values of $K$ and $R^2$ at an optimum pH of 5 are equal to 0.9152 and 0.0167, respectively. Therefore, as the obtained results well fitted and $R^2$ gets closer to 1, the kinetic model of naphthalene removal using this photocatalyst follows second-order kinetics. The kinetics graphs of naphthalene removal in 1/$C$ vs. irradiation time are shown in Figs. 9, 11, and 16. The rate constants were found from the slope of the line 1/$C$ vs. time. The regression coefficient of $R^2$ was greater than 0.9 for the second-order kinetic plot. It should be noted that in this study, the total time of naphthalene compound removal is 90 min. It is clear because the pattern of naphthalene adsorption is completely lost within 90 min and after this time the absorption spectrum is characteristic of the quinoline compound as intermediate resulting from photodegradation of naphthalene. So, the kinetic reaction of naphthalene was analyzed from 0 to 90 min, which was estimated according to the second-order kinetics. A lot of researchers have recorded the kinetics of the photo-oxidation degradation of naphthalene during degradation time of naphthalene, and they report that they follow the first-order kinetics [61,83,84].

### 3.7. Reusability of the catalyst

The reusability of $TiO_2$–N–S was tested for the degradation of naphthalene at an initial concentration of 15 mg/L in the presence of visible and sunlight. After complete degradation, the catalyst was alienated and rinsed with a bulky amount of deionized water. Using a hot air oven, the improved catalyst was dried at 100°C for 90 min and used for a second run. Fig. 18 shows the results of naphthalene degradation for six runs. $TiO_2$–N–S exhibits amazing photostability as naphthalene degradation percentages under visible light are 87.04%, 86.17%, 84.38%, 84.28%, 84.17%, and 84.16% and naphthalene degradation percentages under sunlight are 87.74%, 86.64%, 86.18%, 86.09%, 85.12%, and 85.12% for 90 min in the 1st, 2nd, 3rd, 4th, 5th, and 6th runs, respectively. No significant change was observed in reused $TiO_2$–N–S photocatalyst and it did not change during the reaction, representing the stability of photocatalyst. After the completion of the degradation reaction, the solution was tested for $Ti^{3+}$ leaching with sodium sulfide. There is no precipitation of titanium sulfide (black color) [85], indicating that the catalyst is non-hazardous for aqueous environments.

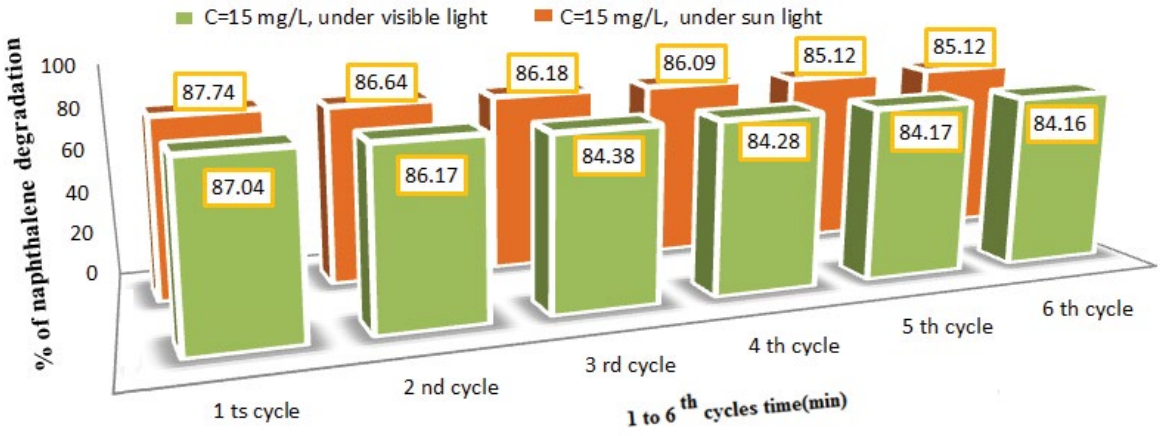


Fig. 18. Reusability the catalyst $TiO_2$–N–S of the solution naphthalene at a concentration of 15 mg/L in the presence of visible and sunlight at 90 min.

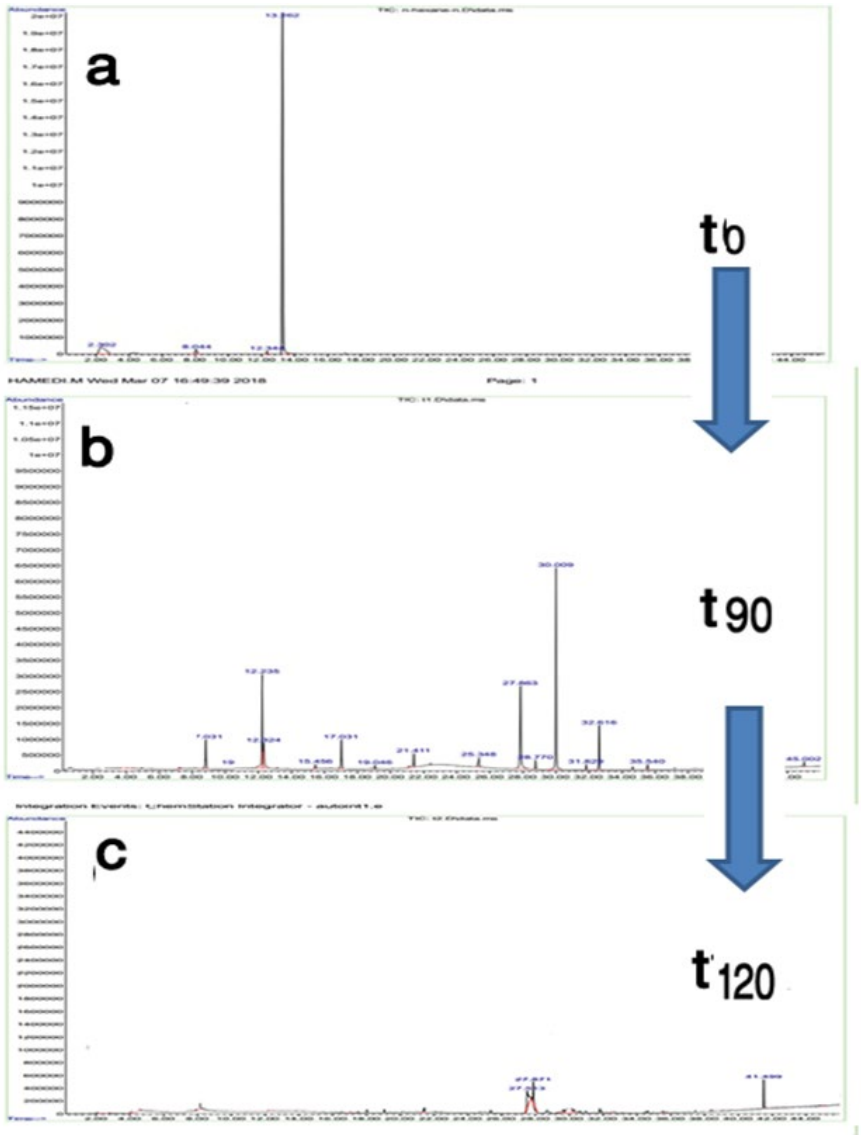


Fig. 19. (a) GC spectrum of pure naphthalene, (b) GC spectrum of solution after 90 min radiation, and (c) GC spectrum of solution after 120 min radiation.

### *3.8. Intermediate compounds produced by naphthalene degradation*

In order to assess the intermediate compounds obtained from the process of photooxidation degradation of naphthalene by $TiO_2$–N–S photocatalyst, Agilent 5975C model GC–MS was used. As the assessment at UV-Vis spectrum indicates that the absorption spectrum of naphthalene is completely removed and another absorption peak emerges at time of 90 min, in order to detect the intermediate compounds produced by degradation at the time of 90 min of radiation in the presence of catalyst, the sample was injected to GC–MS after being extracted by dichloromethane solvent.

Fig. 19 show GC spectrum of the intermediate compounds produced from naphthalene photooxidation by $TiO_2$–N–S catalyst during irradiation. According to retention time and library assessment of device from mass spectrum interpretation, the intermediate compounds include compound 9 (Phthalic acid), compound 15 (2-formyl cinnamaldehyde), compound 16 (2-carboxy-cinamaldehyde), and compound 10 (ethanoic acid), and the proposed mechanism for naphthalene removal is oxidation in the presence of OH radicals and $HO_2$ radicals (Fig. 20). It should be noted that in the previous research, the intermediate compounds produced by naphthalene's photo-oxidation degradation and degradation mechanisms were presented which are in agreement with the results of this study [86,87].

Results from GC–MS assessment of solution after 120 min radiation indicate the removal of intermediates, and finally, mineralization phenomenon of intermediate organic compounds and their conversion into $CO_2$ and $H_2O$ gases, confirming that no absorption spectrum of organic intermediates produced from photo-oxidation is observed after 120 min (Fig. 20c).

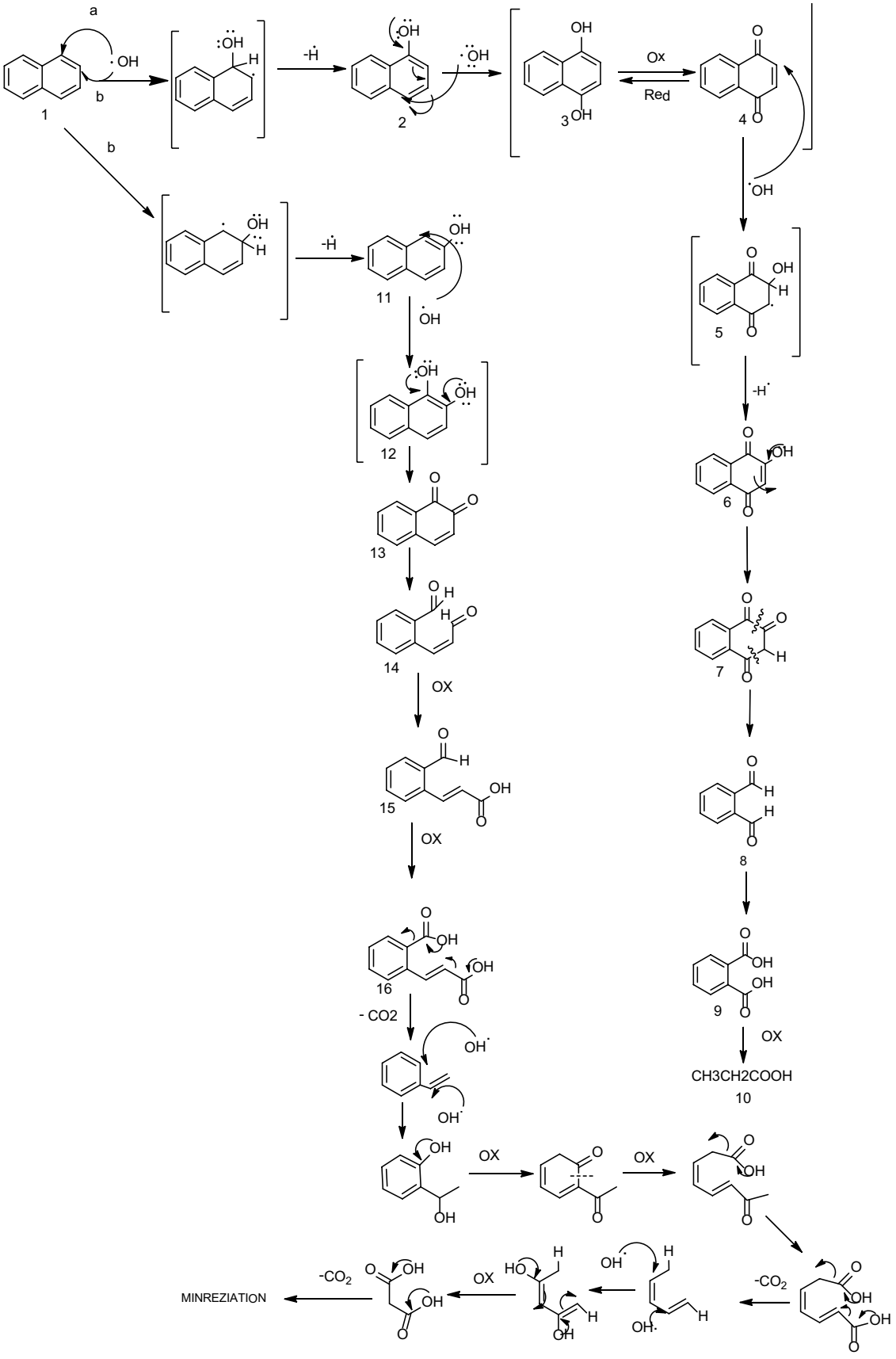


Fig. 20. Intermediate compounds produced from naphthalene photooxidation by $TiO_2$–N–S catalyst.

## 4. Conclusion

In the current research, $TiO_2$ and $TiO_2$–N–S thin film synthesis and deposition on glass microspheres were successfully realized using sol–gel method. The results of XRD analysis of doped samples by two non-metal elements of sulfur and nitrogen and the spectrum of $TiO_2$–N–S nanoparticles formed at 500°C for 1 h showed only the presence of anatase phase and indicated the reduction in nanoparticles size. SEM results showed that the nano size of $TiO_2$–N–S thin film particles is about 10–15 nm. Additionally, results of DRS and FT-IR analyses of samples showed that the energy gap has reduced from 3.2 to 2.98 eV. They showed that the energy gap band has become narrower and the optical activity of $TiO_2$–N–S thin film on glass microspheres has directed toward visible light. The analysis results of naphthalene samples at different concentrations in the presence of visible and sunlight showed that the kinetic equation of naphthalene removal obeys second-order model, and the optimal conditions of naphthalene removal occur at pH = 5 and within 90 min, and an increase in the initial concentration of the solution causes an increase in naphthalene removal efficiency on the same conditions. By increasing the initial concentration of naphthalene from 5 to 25 mg/L at a contact time of 90 min, in the presence of visible light, the removal efficiency increased from 79.04% to 94.28%. The maximum removal efficiency of naphthalene in the presence of visible and sunlight was obtained at a concentration of 25 and 40 mg/L, respectively. GC/MS analysis results showed that at the optimal time of removal (90 min), some intermediate compounds are produced and theses intermediates are converted into water and carbon after another 30 min contact time and the aquatic environment becomes devoid of any organic compound. As a result of using this method in a full scale, it is required to keep contact time up to 120 min. Considering the desirable results of the photocatalytic removal of naphthalene process using nanoparticles synthesized by N and S-doped $TiO_2$ through sol–gel method, it is suggested that the efficiency of this method for removal of the total PAHs is investigated to determine the scope of this process performance with regard to its capability to be used for water treatment and treatment of wastewater containing oil pollutants.

## Acknowledgment

The authors would like to take this opportunity to thank the Head and Personnel of the Water and Wastewater Company of Chaharmahal and Bakhtiari Province (Iran) for their support and assistance during this research project.

## References

[1] H. Muthukumar, A. Gire, M. Kumari, M. Manickam, Biogenic synthesis of nano-biomaterial for toxic naphthalene photocatalytic degradation optimization and kinetics studies, Int. Biodeterior. Biodegrad., 119 (2017) 587–594.
[2] T. Rengarajan, P. Rajendran, N. Nandakumar, B. Lokeshkumar, P. Rajendran, I. Nishigaki, Exposure to polycyclic aromatic hydrocarbons with special focus on cancer, Asian Pac. J. Trop. Biomed., 5 (2015) 182–189.
[3] C. Liu, L. Zhang, R. Liu, Z. Gao, X. Yang, Z. Tu, F. Yang, Z. Ye, L. Cui, C. Xu, Y. Li, Hydrothermal synthesis of N-doped $TiO_2$ nanowires and N-doped graphene heterostructures with enhanced photocatalytic properties, J. Alloys Compd., 656 (2016) 24–32.
[4] F.Y. Griego, K.T. Bogen, P.S. Price, D.L. Weed, Exposure, epidemiology and human cancer incidence of naphthalene, Regul. Toxicol. Pharmacol., 51 (2008) 22–26.
[5] K.H. Kim, S.A. Jahan, E. Kabir, R.J.C. Brown, A review of airborne polycyclic aromatic hydrocarbons (PAHs) and their human health effects, Environ. Int., 60 (2013) 71–80.
[6] S. Baran, P. Oleszczuk, E. Baranowska, Degradation of soil environment in the post-flooding area: content of polycyclic aromatic hydrocarbons (PAHs) and S-triazine herbicides, J. Environ. Sci. Health Part B, 38 (2003) 799–812.
[7] W.F.M. Röling, I.M. Head, S.R. Larter, The microbiology of hydrocarbon degradation in subsurface petroleum reservoirs: perspectives and prospects, Res. Microbiol., 154 (2003) 321–328.
[8] S. Guha, C.A. Peters, P.R. Jaffé, Multisubstrate biodegradation kinetics of naphthalene, phenanthrene, and pyrene mixtures, Biotechnol. Bioeng., 65 (1999) 491–499.
[9] A. Rubio-Clemente, R.A. Torres-Palma, G.A. Peñuela, Removal of polycyclic aromatic hydrocarbons in aqueous environment by chemical treatments: a review, Sci. Total Environ., 478 (2014) 201–225.
[10] R. Raei, M. Ebnali-Heidari, H. Saghaei, Supercontinuum generation in organic liquid–liquid core-cladding photonic crystal fiber in visible and near-infrared regions: publisher's note, J. Opt. Soc. Am. B, 35 (2018) 1545.
[11] H.K. Bojes, P.G. Pope, Characterization of EPA's 16 priority pollutant polycyclic aromatic hydrocarbons (PAHs) in tank bottom solids and associated contaminated soils at oil exploration and production sites in Texas, Regul. Toxicol. Pharmacol., 47 (2007) 288–295.
[12] A.M.J. Law, M.D. Aitken, Bacterial chemotaxis to naphthalene desorbing from a nonaqueous liquid, Appl. Environ. Microbiol., 69 (2003) 5968–5973.
[13] H. Gupta, B. Gupta, Adsorption of polycyclic aromatic hydrocarbons on banana peel activated carbon, Desal. Water Treat., 57 (2016) 9498–9509.
[14] S. Paria, P.K. Yuet, Adsorption of non-ionic surfactants onto sand and its importance in naphthalene removal, Ind. Eng. Chem. Res., 46 (2007) 108–113.
[15] L. Devi, K.J. Ptasinski, F.J.J.G. Janssen, Pretreated olivine as tar removal catalyst for biomass gasifiers: investigation using naphthalene as model biomass tar, Fuel Process. Technol., 86 (2005) 707–730.
[16] T. Benabdallah El-Hadj, J. Dosta, R. Márquez-Serrano, J. Mata-Álvarez, Effect of ultrasound pretreatment in mesophilic and thermophilic anaerobic digestion with emphasis on naphthalene and pyrene removal, Water Res., 41 (2007) 87–94.
[17] K.J. Rockne, S.E. Strand, Anaerobic biodegradation of naphthalene, phenanthrene, and biphenyl by a denitrifying enrichment culture, Water Res., 35 (2001) 291–299.
[18] S. Lamichhane, K.C. Bal Krishna, R. Sarukkalige, Polycyclic aromatic hydrocarbons (PAHs) removal by sorption: a review, Chemosphere, 148 (2016) 336–353.
[19] B. Ma, X. Lv, Y. He, J. Xu, Assessing adsorption of polycyclic aromatic hydrocarbons on *Rhizopus oryzae* cell wall components with water-methanol cosolvent model, Ecotoxicol. Environ. Saf., 125 (2016) 55–60.
[20] C.H. Chiou, R.S. Juang, Photocatalytic degradation of phenol in aqueous solutions by Pr-doped $TiO_2$ nanoparticles, J. Hazard. Mater., 149 (2007) 1–7.
[21] G. Laera, B. Jin, H. Zhu, A. Lopez, Photocatalytic activity of $TiO_2$ nanofibers in simulated and real municipal effluents, Catal. Today, 161 (2011) 147–152.
[22] C.O. Ania, T.J. Bandosz, Importance of structural and chemical heterogeneity of activated carbon surfaces for adsorption of dibenzothiophene, Langmuir, 21 (2005) 7752–7759.
[23] E.W. Rice, R.B. Baird, A.D. Eaton, L.S. Clesceri, Standard Methods for the Examination of Water and Wastewater, American Public Health Association, Washington, DC, USA, 2012.
[24] B. Latkowska, J. Figa, Cyanide removal from industrial wastewaters, J. Environ. Stud., 16 (2007) 148–152.

[25] S. Murgolo, F. Petronella, R. Ciannarella, R. Comparelli, A. Agostiano, M.L. Curri, G. Mascolo, UV and solar-based photocatalytic degradation of organic pollutants by nano-sized $TiO_2$ grown on carbon nanotubes, Catal. Today, 240 (2015) 114–124.
[26] H. Zangeneh, A.A.L. Zinatizadeh, M. Habibi, M. Akia, M. Hasnain Isa, Photocatalytic oxidation of organic dyes and pollutants in wastewater using different modified titanium dioxides: a comparative review, J. Ind. Eng. Chem., 26 (2015) 1–36.
[27] H. Saghaei, M. Ebnali-Heidari, M.K. Moravvej-Farshi, Mid-infrared supercontinuum generation via $As_2Se_3$ chalcogenide photonic crystal fibers, Appl. Opt., 54 (2015) 2072–2079.
[28] H. Saghaei, M.K. Moravvej-Farshi, M. Ebnali-Heidari, M.N. Moghadasi, Ultra-wide mid-infrared supercontinuum generation in $As_{40}Se_{60}$ chalcogenide fibers: solid core PCF versus SIF, IEEE J. Sel. Top. Quantum Electron., 22 (2016).
[29] H. Saghaei, Dispersion-engineered microstructured optical fiber for mid-infrared supercontinuum generation, Appl. Opt., 57 (2018) 5591–5598.
[30] M. Ebnali-Heidari, H. Saghaei, F. Koohi-Kamali, M. Naser Moghadasi, M.K. Moravvej-Farshi, Proposal for supercontinuum generation by optofluidic infiltrated photonic crystal fibers, IEEE J. Sel. Top. Quantum Electron., 20 (2014) 582–589.
[31] H. Saghaei, V. Heidari, M. Ebnali-Heidari, M.R. Yazdani, A systematic study of linear and nonlinear properties of photonic crystal fibers, Optik, 127 (2016) 11938–11947.
[32] J.A. Pedraza-Avella, P. Acevedo-Peña, J.E. Pedraza-Rosas, Photocatalytic oxidation of cyanide on $TiO_2$: an electrochemical approach, Catal. Today, 133–135 (2008) 611–618.
[33] R.M. Mohamed, I.A. Mkhalid, The effect of rare earth dopants on the structure, surface texture and photocatalytic properties of $TiO_2$-$SiO_2$ prepared by sol-gel method, J. Alloys Compd., 501 (2010) 143–147.
[34] M. Kalantari, A. Karimkhani, H. Saghaei, Ultra-wide mid-IR supercontinuum generation in $As_2S_3$ photonic crystal fiber by rods filling technique, Optik, 158 (2018) 142–151.
[35] H. Saghaei, Supercontinuum source for dense wavelength division multiplexing in square photonic crystal fiber via fluidic infiltration approach, Radioengineering, 26 (2017) 16–22.
[36] A. Bozzi, I. Guasaquillo, J. Kiwi, Accelerated removal of cyanides from industrial effluents by supported $TiO_2$ photo-catalysts, Appl. Catal., B, 51 (2004) 203–211.
[37] J. Fan, Z. Zhao, W. Liu, Y. Xue, S. Yin, Solvothermal synthesis of different phase N-$TiO_2$ and their kinetics, isotherm and thermodynamic studies on the adsorption of methyl orange, J. Colloid Interface Sci., 470 (2016) 229–236.
[38] X.F. Lei, X.X. Xue, H. Yang, C. Chen, X. Li, J.X. Pei, M.C. Niu, Y.T. Yang, X.Y. Gao, Visible light-responded C, N and S co-doped anatase $TiO_2$ for photocatalytic reduction of Cr(VI), J. Alloys Compd., 646 (2015) 541–549.
[39] A. Khalilzadeh, S. Fatemi, Modification of nano-$TiO_2$ by doping with nitrogen and fluorine and study acetaldehyde removal under visible light irradiation, Clean Technol. Environ. Policy, 16 (2014) 629–636.
[40] R. Fagan, D.E. McCormack, S. Hinder, S.C. Pillai, Improved high temperature stability of anatase $TiO_2$ photocatalysts by N, F, P co-doping, Mater. Des., 96 (2016) 44–53.
[41] K.P. Priyanka, V.R. Revathy, P. Rosmin, B. Thrivedu, K.M. Elsa, J. Nimmymol, K.M. Balakrishna, T. Varghese, Influence of la doping on structural and optical properties of $TiO_2$ nanocrystals, Mater. Charact., 113 (2016) 144–151.
[42] E.G. Villabona-Leal, J.P. López-Neira, J.A. Pedraza-Avella, E. Pérez, O. Meza, Screening of factors influencing the photocatalytic activity of $TiO_2$:Ln (Ln = La, Ce, Pr, Nd, Sm, Eu and Gd) in the degradation of dyes, Comput. Mater. Sci., 107 (2015) 48–53.
[43] L. Elsellami, H. Lachheb, A. Houas, Synthesis, characterization and photocatalytic activity of Li-, Cd-, and La-doped $TiO_2$, Mater. Sci. Semicond. Process., 36 (2015) 103–114.
[44] L. Yu, X. Yang, J. He, Y. He, D. Wang, Synthesis of magnetically separable N, La-doped $TiO_2$ with enhanced photocatalytic activity, Sep. Purif. Technol., 144 (2015) 107–113.
[45] L. Yu, X. Yang, J. He, Y. He, D. Wang, One-step hydrothermal method to prepare nitrogen and lanthanum co-doped $TiO_2$ nanocrystals with exposed {0 0 1} facets and study on their photocatalytic activities in visible light, J. Alloys Compd., 637 (2015) 308–314.
[46] J. Zhang, L.J. Xu, Z.Q. Zhu, Q.J. Liu, Synthesis and properties of (Yb, N)-$TiO_2$ photocatalyst for degradation of methylene blue (MB) under visible light irradiation, Mater. Res. Bull., 70 (2015) 358–364.
[47] A. Ghanbari, A. Kashaninia, A. Sadr, H. Saghaei, Supercontinuum generation with femtosecond optical pulse compression in silicon photonic crystal fibers at 2500 nm, Opt. Quantum Electron., 50 (2018) 411–422.
[48] H. Saghaei, A. Ghanbari, White light generation using photonic crystal fiber with sub-micron circular lattice, J. Electr. Eng., 68 (2017) 282–289.
[49] A. Ghanbari, A. Kashani Nia, A. Sadr, H. Saghaei, A comparative study of multipole and empirical relations methods for effective index and dispersion calculations of silica-based photonic crystal fibers, J. Commun. Eng., 8 (2019) 98–109.
[50] P. Nickels, H. Zhou, S.N. Basahel, A.Y. Obaid, T.T. Ali, A.A. Al-Ghamdi, E.S.H. El-Mossalamy, A.O. Alyoubi, S.A. Lynch, Laboratory scale water circuit including a photocatalytic reactor and a portable in-stream sensor to monitor pollutant degradation, Ind. Eng. Chem. Res., 51 (2012) 3301–3308.
[51] G. Odling, Z.Y. Pong, G. Gilfillan, C.R. Pulham, N. Robertson, Bismuth titanate modified and immobilized $TiO_2$ photocatalysts for water purification: broad pollutant scope, ease of re-use and mechanistic studies, Environ. Sci. Water Res. Technol., 4 (2018) 2170–2178.
[52] X. Meng, Z. Zhang, Experimental analysis of a photoreactor packed with Pd-$BiVO_4$-coated glass beads, AIChE J., 65 (2019) 132–139.
[53] H. Saghaei, V. Van, Broadband mid-infrared supercontinuum generation in dispersion-engineered silicon-on-insulator waveguide, J. Opt. Soc. Am. B, 36 (2019) A193–A202.
[54] M.A. Rauf, M.A. Meetani, S. Hisaindee, An overview on the photocatalytic degradation of azo dyes in the presence of $TiO_2$ doped with selective transition metals, Desalination, 276 (2011) 13–27.
[55] C.D. Theerakarunwong, S. Phanichphant, Visible-light-induced photocatalytic degradation of PAH-contaminated soil and their pathways by Fe-doped $TiO_2$ nanocatalyst, Water Air Soil Pollut., (2018) 291–229.
[56] O.T. Woo, W.K. Chung, K.H. Wong, A.T. Chow, P.K. Wong, Photocatalytic oxidation of polycyclic aromatic hydrocarbons: intermediates identification and toxicity testing, J. Hazard. Mater., 168 (2009) 1192–1199.
[57] B.J. McConkey, L.M. Hewitt, D.G. Dixon, B.M. Greenberg, Natural sunlight induced photooxidation of naphthalene in aqueous solution, Water Air Soil Pollut., 136 (2002) 347–359.
[58] E.S. Baeissa, Synthesis and characterization of sulfur-titanium dioxide nanocomposites for photocatalytic oxidation of cyanide using visible light irradiation, Chin. J. Catal., 36 (2015) 698–704.
[59] F. Mohammadi-Moghadam, M. Sadeghi, N. Masoudipour, Degradation of cyanide using stabilized S, N-$TiO_2$ nanoparticles by visible and sun light, J. Adv. Oxid. Technol., 21 (2018) 274–284.
[60] M. Farrokhi, J.K. Yang, S.M. Lee, M. Shirzad-Siboni, Effect of organic matter on cyanide removal by illuminated titanium dioxide or zinc oxide nanoparticles, J. Environ. Health Sci. Eng., 11 (2013) 23.
[61] R. Abu-Elella, M.E. Ossman, M. Abd-Elfatah, A. Elgendi, Kinetic modeling and isotherm study for naphthalene adsorption on boehmite nanopowder, Desal. Water Treat., 51 (2013) 3472–3481.
[62] M. Abouseoud, A. Yataghene, A. Amrane, R. Maachi, Effect of pH and salinity on the emulsifying capacity and naphthalene solubility of a biosurfactant produced by *Pseudomonas fluorescens*, J. Hazard. Mater., 180 (2010) 131–136.
[63] A.A. Tabrizi, A. Pahlavan, Efficiency improvement of a silicon-based thin-film solar cell using plasmonic silver nanoparticles and an antireflective layer, Opt. Commun., 454 (2020) 124437.

[64] V. Mahmoodi, J. Sargolzaei, Photocatalytic abatement of naphthalene catalyzed by nanosized $TiO_2$ particles: assessment of operational parameters, Theor. Found. Chem. Eng., 48 (2014) 656–666.
[65] M. Sathish, R.P. Viswanath, C.S. Gopinath, N,S-Co-doped $TiO_2$ nanophotocatalyst: synthesis, electronic structure and photocatalysis, J. Nanosci. Nanotechnol., 9 (2009) 423–432.
[66] A. Brindha, T. Sivakumar, Visible active N, S co-doped $TiO_2$/graphene photocatalysts for the degradation of hazardous dyes, J. Photochem. Photobiol. A, 340 (2017) 146–156.
[67] Y.H. Lin, H.T. Hsueh, C.W. Chang, H. Chu, The visible light-driven photodegradation of dimethyl sulfide on S-doped $TiO_2$: characterization, kinetics, reaction pathways, Appl. Catal., B, 199 (2016) 1–10.
[68] D. Liu, Z. Wu, X. Ge, G. Cravotto, Z. Wu, Y. Yan, Comparative study of naphthalene adsorption on activated carbon prepared by microwave-assisted synthesis from different typical coals in Xinjiang, J. Taiwan Inst. Chem. Eng., 59 (2016) 563–568.
[69] B. Qiu, M. Xing, J. Zhang, Mesoporous $TiO_2$ nanocrystals grown in situ on graphene aerogels for high photocatalysis and lithium-ion batteries, J. Am. Chem. Soc., 136 (2014) 5852–5855.
[70] R. López, R. Gómez, Band-gap energy estimation from diffuse reflectance measurements on sol–gel and commercial $TiO_2$: a comparative study, J. Sol-Gel Sci. Technol., 61 (2012) 1–7.
[71] Sutisna, M. Rokhmat, E. Wibowo, Khairurrijal, M. Abdullah, Prototype of a flat-panel photoreactor using $TiO_2$ nanoparticles coated on transparent granules for the degradation of Methylene Blue under solar illumination, Sustainable Environ. Res., 27 (2017) 172–180.
[72] N. Masoudipour, M. Sadeghi, F. Mohammadi-Moghadam, Photo-catalytic inactivation of *E. coli* using stabilized Ag/S, N-$TiO_2$ nanoparticles by fixed bed photo-reactor under visible light and sunlight, Desal. Water Treat.m 110 (2018) 109–116.
[73] J. Wang, H. Li, H. Li, C. Zou, Mesoporous $TiO_2$-xAy (A = N, S) as a visible-light-response photocatalyst, Solid State Sci., 12 (2010) 490–497.
[74] F. Zhang, J. Zhao, T. Shen, H. Hidaka, E. Pelizzetti, N. Serpone, $TiO_2$-assisted photodegradation of dye pollutants II. Adsorption and degradation kinetics of eosin in $TiO_2$ dispersions under visible light irradiation, Appl. Catal., B, 15 (1998) 147–156.
[75] X. Quan, X. Zhao, S. Chen, H. Zhao, J. Chen, Y. Zhao, Enhancement of p,p′-DDT photodegradation on soil surfaces using $TiO_2$ induced by UV-light, Chemosphere, 60 (2005) 266–273.
[76] H. Zhao, S. Xu, J. Zhong, X. Bao, Kinetic study on the photo-catalytic degradation of pyridine in $TiO_2$ suspension systems, Catal. Today, 93–95 (2004) 857–861.
[77] S. Chaudhary, P. Sharma, A. Kaur, R. Kumar, S.K. Mehta, Surfactant coated silica nanoparticles as smart scavengers for adsorptive removal of naphthalene, J. Nanosci. Nanotechnol., 18 (2017) 3218–3229.
[78] D. Avisar, Y. Lester, H. Mamane, pH induced polychromatic UV treatment for the removal of a mixture of SMX, OTC and CIP from water, J. Hazard. Mater., 175 (2010) 1068–1074.
[79] A.G. Rincón, C. Pulgarin, Effect of pH, inorganic ions, organic matter and $H_2O_2$ on *E. coli* K12 photocatalytic inactivation by $TiO_2$: implications in solar water disinfection, Appl. Catal., B, 51 (2004) 283–302.
[80] J.M. Pettibone, D.M. Cwiertny, M. Scherer, V.H. Grassian, Adsorption of organic acids on $TiO_2$ nanoparticles: effects of pH, nanoparticle size, nanoparticle aggregation, Langmuir, 24 (2008) 6659–6667.
[81] M. Muruganandham, M. Swaminathan, Advanced oxidative decolourisation of Reactive Yellow 14 azo dye by UV/$TiO_2$, UV/$H_2O_2$, UV/$H_2O_2$/$Fe^{2+}$ processes - A comparative study, Sep. Purif. Technol., 48 (2006) 297–303.
[82] H.G. Yang, C.H. Sun, S.Z. Qiao, J. Zou, G. Liu, S.C. Smith, H.M. Cheng, G.Q. Lu, Anatase $TiO_2$ single crystals with a large percentage of reactive facets, Nature, 453 (2008) 638–641.
[83] L. Yang, X. Qian, Z. Wang, Y. Li, H. Bai, H. Li, Steel slag as low-cost adsorbent for the removal of phenanthrene and naphthalene, Adsorpt. Sci. Technol., 36 (2018) 1160–1177.
[84] P. Das, S. Goswami, S. Maity, Removal of naphthalene present in synthetic waste water using novel G/GO nano sheet synthesized from rice straw: comparative analysis, isotherm and kinetics, Front. Nanosci. Nanotechnol., 2 (2016) 38–42.
[85] J. Kamalakkannan, V.L. Chandraboss, S. Prabha, S. Senthilvelan, Activated carbon loaded N, S co-doped $TiO_2$ nanomaterial and its dye wastewater treatment, Int. Lett. Chem. Phys. Astron., 47 (2015) 147–164.
[86] M.J. García-Martínez, L. Canoira, G. Blázquez, I. Da Riva, R. Alcántara, J.F. Llamas, Continuous photode,gradation of naphthalene in water catalyzed by $TiO_2$ supported on glass Raschig rings, Chem. Eng. J., 110 (2005) 123–128.
[87] L. Hykrdová, J. Jirkovský, G. Mailhot, M. Bolte, Fe(III) photoinduced and Q-$TiO_2$ photocatalysed degradation of naphthalene: comparison of kinetics and proposal of mechanism, J. Photochem. Photobiol. A, 151 (2002) 181–193.